Three Dimensional Measurements of Pore Morphological and Hydraulic Properties

Hyen-Chung Chun, Daniel Gimenez[1], Sung-Won Yoon[2], Richard Heck[3], Tom Elliot[3],

Laise Ziska[4], Kate Geaorge[4], Yeon-Kyu Sonn, and Sang-Keun Ha*

National Academy of Agricultural Science, Rural Development Administration, Suwon 441-707, Korea

[1]*Department of Environmental Sciences, Rutgers, The State University of New Jersey,*

14 College Farm Road · New Brunswick, NJ 08901

[2]*National Institute for Agronomic Research, France*

[3]*Department of Land Resource Science, Ontario Agricultural College, University of Guelph,*

Guelph, Ontario, Canada N1G 2W1

[4]*Agricultural Research Services, 10300 Baltimore Avenue Building 001 Beltsville, Maryland, 20705-2350*

Pore network models are useful tools to investigate soil pore geometry. These models provide quantitative information of pore geometry from 3D images. This study presents a pore network model to quantify pore structure and hydraulic characteristics. The objectives of this work were to apply the pore network model to characterize pore structure from large images to quantify pore structure, calculate water retention and hydraulic conductivity properties from a three dimensional soil image, and to combine measured hydraulic properties from experiments with calculated hydraulic properties from image. Soil samples were taken from a site located at the Baltimore science center, which is located inside of the city. Undisturbed columns were taken from the site and scanned with a computer tomographer at resolutions of 22 μm. Pore networks were extracted by medial-axis transformation and were used to measure pore geometry from one of the scanned samples. Water retention and unsaturated hydraulic conductivity values were calculated from the soil image. Properties of soil bulk density, water retention and unsaturated hydraulic conductivity were measured from three replicates of scanned soil samples. 3D image analysis provided accurate detailed pore properties such as individual pore volumes, pore length, and tortuosity of all pores. These data made possible to calculate accurate estimations of water retention and hydraulic conductivity. Combination of the calculated and measured hydraulic properties gave more accurate information on pore sizes over wider range than measured or calculated data alone. We could conclude that the hydraulic property computed from soil images and laboratory measurements can describe a full structure of intra- and inter-aggregate pores in soil.

Key words: pore geometry, computer tomography, medial axis model, water retention, unsaturated hydraulic conductivity

Introduction

Soil pore size and shape influence soil water transport/ biological processes, therefore quantification of these properties is important to understand these processes (Leij et al., 2006). Soil pores occur in a wide range of sizes and shapes in nature (Pagliai and Vignozzi, 2002). Pore size distribution is determined by water retention measurements or mercury intrusion porosimetry (Pagliai et al., 1995; Strudley et al. 2008). The equivalent radius of the largest pore that is filled, with water/mercury, is a function of the soil water/mercury pressure through the capillary action. These experimental methods have been developed over decades and are considered good characterizations of soil pore size distributions. However, they cannot provide accurate description of pore sizes, because there can be changes of soil conditions (expansion or shrinkage of the sample) during the measurements (Pires et al., 2005). Recent development of image analyses, especially three dimensional image analyses, makes possible the quan-

tification of pore volumes directly (Peth et al., 2008; Sluetel et al., 2008; Udawatta and Anderson, 2008). Pore sizes or volumes, from three dimensional images are a better measurement of real pores than pore geometry measurements from two dimensional images, since soil pores are in three dimensional in soil (Barstardie et al., 2003). The computer tomography provides the images from which pore volumes can be driven. Slutel et al. (2008) quantified pore volumes with a resolution of 1.7 μm in diameter, while Barstardie et al. (2003) analyzed pores created by earthworms with diameter of up to 10 cm.

The characterization of water movement through soil is important to determine soil quality for agricultural/ environmental management of soil (Strudley et al., 2008). Characterizations of hydraulic properties reflect pore structural characteristics in a soil system (Hayashi et al., 2006). The hydraulic behavior within soils is affected by pore structure and it becomes complicated by the duality of the pore system of large inter-aggregate pores and much finer intra-aggregate pores.

Water retention characteristic curves (WRC) refer to the relation between the matric potential of soil water and volumetric water content (Gimenez et al., 1997). Soil texture and soil structure can affect WRC (Wittmuss and Mazurak, 1958; Tamboli et al., 1964; Amemiya, 1965).

Since three dimensional images can provide pore size distributions, water retention values can be computed inversely from pore size distributions and matric potentials from corresponding pore sizes (Vogel and Roth, 2001). Peth et al. (2008) calculated WRC from aggregate images and found that computed WRC captured different pore systems resulted by different treatments.

Hydraulic conductivity is determined by the ability of the soil fluid to flow through the soil matrix system under a specified hydraulic gradient (Radcliffe and Rasmussen, 2002). The hydraulic conductivity is especially related to inter-aggregate pore conditions (Balland et al., 2008). Under conditions close to saturation, the large inter-aggregate pores form the primary pathways for rapid infiltration. Hydraulic conductivity can also be estimated from three dimensional soil images. Hydraulic conductivity can be calculated with soil water contents and matric potentials (Green and Corey, 1971; Mualem, 1976; Wosten and Van Genuchten, 1988).

The objectives of this study were to characterize soil pore geometry, from a three dimensional image, based on a pore network model, to compute hydraulic properties from the image and to combine measured hydraulic properties from experiments with calculated hydraulic properties from images to describe accurate pore structure.

Materials and Methods

Soils   The site selected for this study was located at the Baltimore science center, which is located inside of the city. In 2002, the top 20 cm of a fallow soil that did not have any fertilizer applications for 5 years was removed from the Beltsville experimental farm over a 6 × 9 m. These soils were sieved to remove rhizomes, stolons and corms, and then mixed uniformly with seeds of 30 plant species. Then from the 6 × 9 m area of the Beltsville experimental farm, soils were excavated up to 110 cm (B and C horizons) and mixed well. Four plots with size of 2 × 2 m were established at the site in 2002. All plots were excavated to a depth of 110 cm and filled with the lower horizon soils first and soils with seeds were placed on top (Ziska et al., 2004). Soil samples were then taken at the site to a depth of 30 cm.

An undisturbed bulk soil (5.5 cm in diameter and 12 cm in height) was sampled from each of the three plots by excavating a sample carefully. The outside of each sample was covered by cheesecloth with saran to harden the surface of the sample. The cheesecloth was soaked lightly to prevent infiltration of saran solution (mixing of saran powder in methyl ethyl keton) into pores, but thickened enough to harden the surface of the sample. In this chapter, one sample from the site was used for image analyses.

Computer Tomography (CT) and Image Processing
An axial X-ray micro computer tomographer (model MS, General Electric Medical Systems, London, ON, Canada) located at the University of Guelph (ON, Canada) was used to scan soil samples. The resolution of the scans was 22 μm for the bulk soil samples. Series of two dimensional cross sectional images were reconstructed into three dimensional images by Microview software (GE Healthcare Biosiences). After reconstruction of three dimensional images, gray images were converted to binary images using a Java program in Image J (Research Services Branch, National Institute of Health, Bethesda, MD) developed by Elliot and Heck (2007).

A Fortran code was written to identify pores and quantify number of pores, pore volumes, number of throats, throat volumes, pore length and tortuosity from

the scanned image. The calculation was based on pore network model developed by Lindquist et al. (1996). Medial-axis skeletonization was applied to extract representative pore geometry and pore networks (Lindquist and Venkatarangan, 1999). This algorithm was derived by finding continuous axes located in the middle of a pore to provide simple and compact geometric information. The first step of medial-axis skeletonization was burning pore pixels. Lindquist and Venkatarangan (1999) explained the burning analogous to fire spreading. If each pore is fired simultaneously all around pore boundary, it will burn toward the center of the pore. As fire moves inside, pore pixels or voxels, which contacted the fire, are assigned burn numbers with increment. Therefore, burn number is the greatest at the center of a pore. A greater maximum burn number means that the pore is larger than a pore with smaller maximum burn number, since it takes longer to reach the center of the pore. Medial-axis (MA) represents skeleton of a pore by connecting center parts of a pore. In geometrical terms, pores are modeled as a relatively large pore-body connected by relatively small throats (Vogel and Roth, 2003). In this study, pore-body and throats were calculated from all individual pores. Based on pore-body and throat identification, volumes, lengths and tortuosities of all pores were quantified.

Bulk Density After scanning the soil samples, the bulk density (ρ_b) was measured by saran resign bulk density procedure (Sheldrick, 1984). The samples were prepared by first, coating the sample with a saran resin. These sample were weighed in air and then in water. The weights before and after dipping in saran and weight after immersed into water were used to calculate actual weight and volumes of the samples.

$$\rho_b = \frac{W}{V}$$ (1)

where ρ_b is the bulk density, W is weight of soil sample and V is volume of soil sample. W was calculated by *(W1-W2/N-1) +W1-W2*, where *W1* is air weight after *N* time dipping into saran and *W2* is air weight before dipping. *V* was calculated by *W1- W3-(W/1.3)*, where *W3* is weight after immersed into water and 1.3 (g cm⁻³) is the density of saran. This measurement was repeated for three replicates of the bulk soil from each site.

The saturated water contents (θ_s) from all samples were calculated from the bulk density results;

$$\theta_s = 1 - \frac{\rho_b}{\rho_p}$$ (2)

where ρ_b is the bulk density and ρ_p is particle density assumed to be equal to 2.65 g/cm³.

Water Retention and Hydraulic Conductivity
Water retention and infiltration rate were measured after measuring bulk density. Each sample was cut into cylindrical shape with 5 cm in diameter and 3 cm in height and flat surfaces at the both ends. One of the ends was placed on top of a ceramic plate contained in a cell designed to measure hydraulic conductivity and soil water retention in the range of the pressure heads between 0 and -10 kPa. Before the samples were placed in the pressure plate extractors, steady-state infiltration rate was measured for all bulk soil samples. The tension disc infiltrometer used in this study from Decagon Devices (Pullman, WA). Five pressure heads of – 0.2, - 0.3, - 0.4, -0.5, and – 0.6 kPa were applied and the steady-state infiltration rates were measured.

Soil water retention for the soil samples was measured at pressure potentials of -0.3, -0.6, -1, -1.5, -3, -6, and -10 kPa. After measuring water retention at -10 kPa, water retention at pressures of -30, -100, and -300 kPa were measured on the samples using pressure plate extractors.

Water retention was also computed from pore size distributions for the bulk soil images by assuming that pores hold water inside with capillary force and matric potential ψ_i was calculated with corresponding pore radii r_i, using Young – Laplace equation (Peth et al. 2008):

$$\psi_i = 2\sigma\cos(\omega)r_i^{-1}$$ (3)

Where σ is the interfacial tension between air and water (72.7 ×10-3 N m⁻¹) and ω is the contact angle assumed to be 0. At each potential, pores whose radii are smaller than the radius corresponding to the potential are saturated. This water content value at each potential was divided by the image volume. Since the measured water retention data were calculated by gravimetric water content, computed water retention data were divided by the average bulk density of each soil. If a pore had throats, smallest throat radius was applied to Eq. 3 instead of whole pore volume. The computed data were matched to

the measured water retention. In the matching process, the highest matric potential from images was about -0.3 kPa. Therefore water contents at -0.3 kPa from images and average water content at -0.3 kPa from measurements were assumed as the same value of water retention. Water retention contents from images at greater matric potentials were added to the retention value at -0.3 kPa.

Unsaturated hydraulic conductivity was calculated as according to Green and Corey, (1971);

$$K(\theta) = \frac{K_s}{K_{sc}} \cdot \frac{30 \, r^2}{\rho_w \cdot g \cdot \eta} \cdot \frac{\varepsilon^\tau}{\mathrm{n}^2} \sum [(2j+1+2i)\psi_j^{-2}]$$

(4)

where $K(\theta)$ is the calculated conductivity for a specified water content or pressure (m s^{-1}), θ is the water content (m^3 m^{-3}), i denotes the last water content class, ρ_w is the density of water (kg m^{-3}), g is the gravitational constant (m s^{-2}), γ is the viscosity of water (kg m^{-1} s^{-1}), ε is the porosity (m^3 m^{-3}) or water content at corresponding potential, τ is a tortuosity parameter, n is the total number of pore classes, ψ_i is the pressureis the pre for the largest pore with water filled by capillary force. The pressure ψ_i corresponding to θ_j was obtained from water retention data. The τ value was calculated as (actual pore length/ shortest length)^2 from each pore. K_s/K_{sc} is the matching factor, where K_s is the measured saturated conductivity and K_{sc} is calculated conductivity. The value of K_s was 0.11 cm min^{-1} for the urban bulk soil and 0.06 cm min^{-1} for the rural bulk soil from infiltration rate measurement at -0.1 kPa. K_{sc} values were calculated from the largest pore in the image of each sample and the urban bulk soil was 0.45 cm min^{-1} and the rural soil was 0.32 cm min^{-1}. The greatest matric potential from the measured conductivity data was -0.2 kPa and the computed conductivity at -0.2 kPa from an image was matched to the one from the measured data at -0.2 kPa.

Statistical Analysis   Average and standard deviations of all properties (except number of pores and coordination numbers) were calculated by geometric mean and geometric standard deviation, since most results exhibited lognormal distribution.

The geometric mean (E) and standard deviation ($StdDev$) was calculated as;

$$E = e^{\mu + \sigma^2/2}$$

(5)

and

$$StdDev = \sqrt{(e^{\sigma^2} - 1)e^{2\mu + \sigma^2}}$$

(6)

where μ and σ are the mean and standard deviation of the natural log transformed variables.

Water retention curves were fitted with the bimodal model of Duner (1994);

$$S_e = v_1 \left[\frac{1}{1 + (\chi_1 \psi)^{n_{11}}} \right]^{m_1} + (1 - v_1) \left[\frac{1}{1 + (\chi_2 \psi)^{n_{12}}} \right]^{m_2}$$

(7)

where S_e is the effective water content, Ψ is matric potential (kPa), and v_1, χ_1 (m^{-1}), χ_2 (m^{-1}), n_1, and n_2 are fitted parameters. The m parameters are determined by $m = (1-1/n)$. The fitting of water retention was done with the "SWRC fit" program developed by Seki (2007) (http://seki. webmasters.gr.jp/swrc/).

The hydraulic conductivity curves ($k(\psi)$) from image analyses and measurements were fitted with the bimodal model of Durner et al. (1999);

$$k(\psi) = \begin{cases} K_s (v_2 S_{e1})^\tau \dfrac{(v_2 \chi_3 [1 - (1 - S_{e1}^{1/m_{21}})^{m_{21}}])^2}{(v_2 \chi_3)^2} & \psi < \psi_b \\[3mm] K_s ((1 - v_2) S_{e2})^\tau \dfrac{(v_3 \chi_4 [1 - (1 - S_{e2}^{1/m_3})^{m}])^2}{(v_3 \chi_4)^2} & \psi_b < \psi \le 0 \end{cases}$$

(8)

where $S_{ei} = [1 + (\alpha_i |\psi|)^{n_i}]^{m_i}$ is the partial saturation of the ith pore system and ψ_b is the matric potential at a breakpoint of different pore systems. The v_2, v_3, χ_1, χ_2, n_3, n_4 and $m_2 = (1-1/n)$ are fitted parameters. The parameter τ is related to tortuosity and average tortuosity results from image analysis were applied to Eq. 8. The fitting was performed with a Fortran program.

Results and Discussion

Morphological properties   The three dimensional images from the scanned soil are displayed in Fig. 1 and 2. The Fig. 1 shows a partial medial axis structure (100 by 100 by 50 pixels equivalent to 2.2 mm by 2.2 mm by 1.1
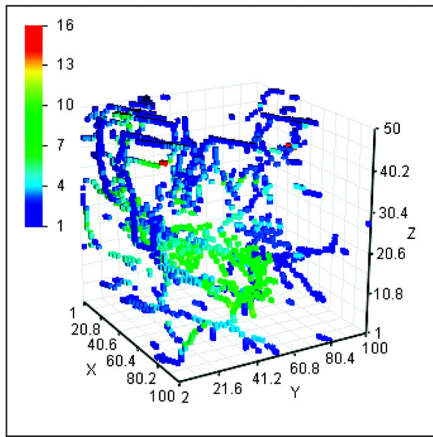
Fig. 1. An example of medial axis construction (burning number) from the soil sample. The legend is the burning numbers to the corresponding pores.
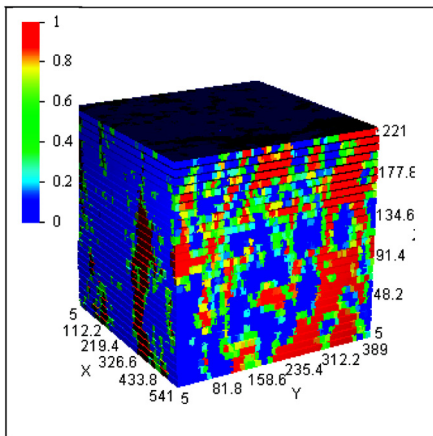

Fig. 2. An example of whole pore structure from the soil sample. The legend is positions of the pore pixels such as more blue color pixels are closer to solid and pores with more red color pixels are closer to the center of the pores.

mm) of the pore structure when the whole scanned image was 1000 by 1000 by 1000 pixels (equivalent to 22 mm by 22 mm by 22 mm). The colors in Fig. 1 represent the burning numbers of pore structure. In other words, greater burning numbers were greater values in sizes. The Fig. 2 shows the whole pore structure of the soil sample. The red area represents the pore areas and the soil sample had relatively large size of pores throughout the sample. All morphological properties obtained from the image were

applied to Eq. 5 and 6 and the average and standard deviation values from all 789 pores are shown in Table 1. The numbers of pores were obtained by counting individual pores. After identifying individual pores, pore-body and throat volumes were quantified (Fig. 3). Pore length and tortuosity were calculated from all pores (Fig. 4 & 5). The soil had pore- body volume range from 0.01 to 218 m m-3, while throat volume ranged from 0.017 to 0.077 m m-3. Pore length was determined by a length from, a medial axis at the top of a pore (closest to surface) to a medial axis at a bottom of a pore. The soil had 74% of pores shorter than 1 mm and the proportion of pores longer than 10 mm was 3%. Tortuosity was a ratio of a shortest or straight length from top to bottom of a pore to an actual pore length calculation. The tortuosity values less than 2 were 72% which meant that there were relatively large size pores (inter-aggregate pores) within the soil. Perret et al. (1999) found that inter-aggregate pores had tortuosity values range from 1 to 2.5 and in this study, the analyzed soil had greater amount of pores with tortuosity values less than 2.

Hydraulic properties   Average bulk densities from three replicates of the samples and the fitted parameters from Eq. 7 and 8 are shown in Table 2. Water retention and
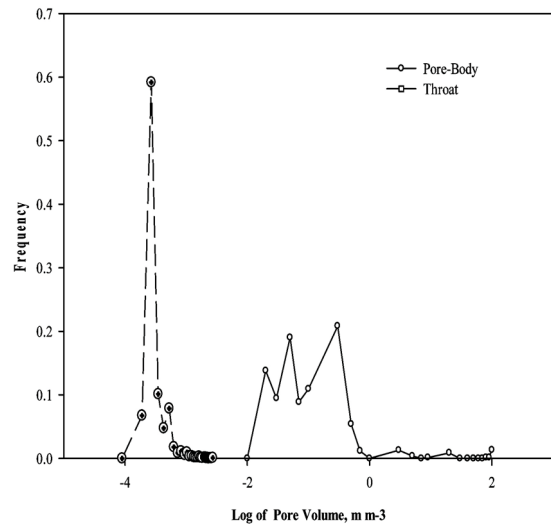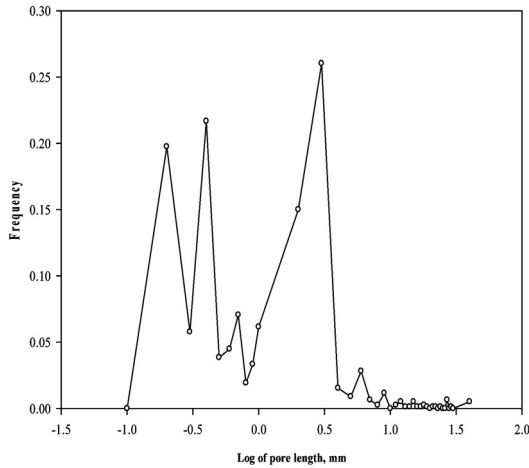

Fig. 3. Frequency distributions of pore-body and throat volumes in logarithm scale from a scanned soil sample.

Table 1. Summary of pore morphological analyses from the soil sample. All properties are presented by average and standard deviation values, except porosity, number of pores and throats.

Porosity	Number of pores	Average pore-body volume (mm^3)	Number of throats	Average throat volume (mm^3)	Pore length (mm)	Tortuosity
0.25	789	0.85±0.16	454	0.21±0.00	1.1±0.36	1.03±0.17

Fig. 4. Frequency distributions of pore lengths in logarithm scale from a scanned soil sample.
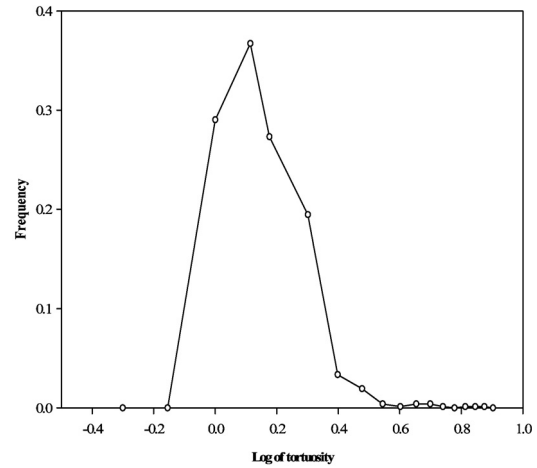
Fig. 5. Frequency distributions of tortuosity in logarithm scale from a scanned soil sample.

hydraulic conductivity were computed from pore size distributions from images. The hydraulic properties depend not only on the pore volume, but also on the continuity of pores (Horn and Smucker, 2005). Water flow in a pore is controlled by throat size instead of pore-body size. Throat and tortuosity results from all samples were applied to water retention and hydraulic

Table 2. Average Bulk density from three bulk soil samples and fitted parameters from water retention (Eq. 7) and conductivity (Eq. 8). θ_s and θr are estimated saturated water content and residual water content from Eq. 7, respectively. Numbers in parenthesis are standard error of fitting.

Bulk density (g cm^{-3})	1.47 ± 0.06
Saturated water content (cm^3 cm^{-3})	0.44 ± 0.02
Water retention fitting (Eq. 7)	
θ_s (cm^3 cm^{-3})	0.57
θ_r (cm^3 cm^{-3})	0.15
v_1	0.29
χ_1	2.67
n_1	4.99
χ_2	0.01
n_2	7.75
Hydraulic conductivity fitting (Eq. 8)	
v_1	0.01
a_1	0.17
n_1	1.01
a_2	0.02
n_2	1.01
Ψ_b (kPa)	-0.3
K_s (cm min^{-1})	0.50

conductivity calculation. Computed water retention data and measured data from laboratory experiments were matched and fitted by Eq. 3 (Fig. 6). There was no information for pores less than 0.1 mm in radius from image analysis due to image resolution and compute limitation. Pore sizes smaller than 22 μm were not scanned or ignored while computations.

There were two distinct curves between the computed water retention curve from images and the measured retention curve from experiments. This implies that the bulk soil samples had dual pore systems (Spohrer et al., 2006). Therefore, a bimodal model (Durner, 1994) fitted the water retention curves reasonably well ($r^2 = 0.99$). The parameters χ_1 and χ_2 from Eq. 7 are scaling factor that indicate the positions of maximum pore size and n_1 and n_2 are related to the width of pore size distribution (Abenny-Mickson, 1996). Pires et al. (2008) compared water retention parameters before and after applying a number of dry-wet cycles. They found that a greater number of dry-wet cycles increased pore size, porosity, and the value of α and n. Hydraulic conductivity distributions were computed from pore radii and water retention data by Eq. 4. Pores with throats and tortuosity values were applied to the calculation to define more accurate estimation of conductivity (Kutilek, 2004) (Fig. 7). Water in a pore with a throat was not released until matric potential was greater than the potential corresponding to throat diameter. In addition, under unsaturated conditions, water in a pore moves along the wall of a pore. Commonly the value of the tortuosity parameter in Eq. 4 was assumed equal to 0.5 based on average tortuostiy values from different texture soils (Mualem, 1976). However, Vervoot and Cattle
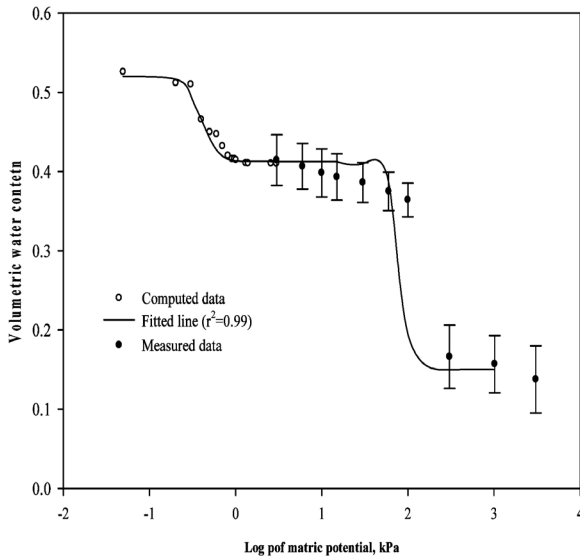
Fig. 6. Computed water retention from a soil and average water retention of measurements data from the three soils and fitted line by Eq. (7). Circle symbols represent data from the soil (empty- computed data and solid-measured data) and solid line is fitted line for the soil.
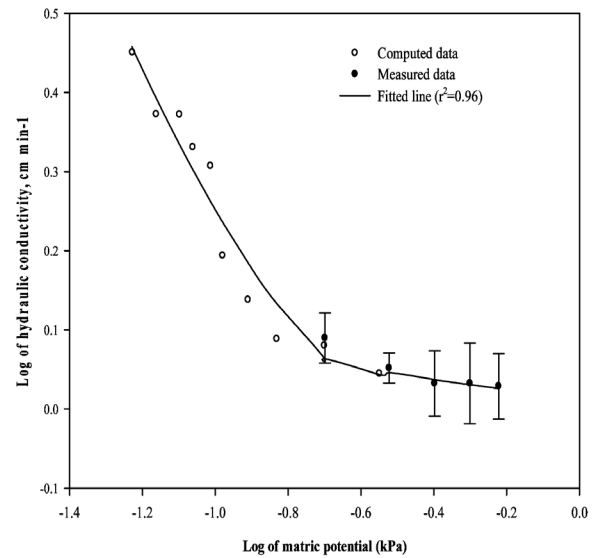
Fig. 7. Computed hydraulic conductivity from a soil and average hydraulic conductivity of measurements data from the three soils and fitted line by Eq. 8. Circle symbols represent data from the urban soil and square symbols do data from the rural soil. Solid line is fitted line for the urban soil and dash line is for the rural soil.

(2003) argued that a constant tortuosity may not correct to predict accurate k_s and recommended to use individual tortuosity from each pore from image analysis of pore geometry. Therefore, throat size and tortuosity data from individual pore were applied to Eq. 4. The fitting for the conductivity curves was done by Eq. 8, which was a bimodal model of a conductivity distribution. Conductivity data from measurements and computed from the image had two different fitting parameters, which were similar to water retention curves. The results of bimodal fitting model suggested that dual porosity system developed in the sample soils. The estimated saturated hydraulic conductivities (k_s) from the sample was greater than measured conductivities by more than 10%. Ventrella et al. (2005) stated that estimated k_s values from Eq. 8 were much greater than the measured values. They stated that estimated values should be treated as a fitting parameter rather than the actual conductivity at saturation, because computed k_s values from conductivity models are not accurate estimation from pore geometry. Other fitted parameters, v_2, v_3, χ_1, χ_2, n_3, and n_4, did not have a similar trend or values in comparison to the parameters from the water retention model.

Traditional hydraulic measurements of soil samples had limitation of obtaining information of intra-aggregate pores, while hydraulic information from the pore network

at a relatively large resolution did not capture properties of intra-aggregate or small size pores.

Conclusion

Soil pore morphological properties have been analyzed from a three dimensional image. Image analysis of three dimensional images of soils is useful to quantify pore properties and characterize pore structure from soils. The medial axis model was able to quantify pore morphological properties from a large size sample or image. The pore network suggested that prediction of hydraulic properties from three dimensional images can be supplementary to laboratory measurements, especially, inter-aggregate pore properties. Combination of hydraulic data from an image and measurement had complete information of inter-aggregate pores and intra-aggregate pores since pores from images were limited by image resolutions and cell sizes and pores from measurement gave inaccurate values for large size pores. This pore network model can be applied to simulation of soil structure. Especially, this model is useful to predict hydraulic properties and inter-aggregate pore properties since the model can preserve large size pore properties and provides quantitative information of pore geometry and related properties. Simulation of pore structure using the

modified pore network model would reveal more detailed information of soil properties as climate change and predict changes of pore properties

References

Abenny-Mickson, S., T. Miura, and A. Yomota. 1996. Evaluation of two soil water retention models for the prediction of hydraulic conductivity of Daisen Kuroboku (volcanic ash) soil. Soil Phys. Cond. Plant Growth Jpn. 74:17−27.

Amemiya, M. 1965. The influence of aggregate size on soil moisture content capillary conductivity relations. Soil Sci. Soc. Am. Proc. 29:744-748.

Balland, V., J.A. P. Pollacco, and P.A. Arp. 2008. Modeling soil hydraulic properties for a wide range of soil conditions. Ecol. Model. 219(3-4): 301-316.

Bastardie, F.Y., Capowiez, J.R. de Dreuzy, and D. Cluzeau. 2003. X-ray tomographic and hydraulic characterization of burrowing by three earthworm species in repacked soil cores. Appl. Soil Ecol. 24(1): 3-16.

Durner, W. 1994. Hydraulic conductivity estimation for soils with heterogeneous pore structure. Water Resour Res. 30:211−33.

Durner, W., E. Priesack, H.J. Vogel, and T. Zurmühl. 1999. Determination of parameters for flexible hydraulic functions by inverse modeling. In: M. Th. van Genuchten, F. J. Leij and L. Wu (eds.) Proc. Int. Workshop, Characterization and Measurement of the Hydraulic Properties of Unsaturated Porous Media. p. 817-830. University of California, Riverside, CA.

Elliot, T. R. and R. J. Heck. 2007 A comparison of optical and X-ray CT technique for void analysis in soil thin section. Geoderma. 141(1-2):60-70.

Gimenez. D., E. Perfect, W.J. Rawls, and Y. Pachepsky. 1997. Fractal models for predicting soil hydraulic properties: a review. Eng Geol. 48 (3-4): 161-183.

Green, R.E. and J.C. Corey. 1971. Calculation of hydraulic conductivity: A further evaluation of some predictive methods. Soil Sci. Soc. Am. Proc. 32(561-565).

Hayashi, Y., K. Ken'ichirou, and T. Mizuyama. 2006. Changes in pore size distribution and hydraulic properties of forest soil resulting from structural development. J. Hydrol. 331: 85− 102.

Horn, R. and A.J.M. Smucker. 2005. Structure formation and its consequences for gas and water transport in unsaturated arable and forest soils. Soil Tillage Res. 82:5−14.

Kutilek, M. 2004. Soil hydraulic properties as related to soil structure. Soil Till. Res. 79: 175-184.

Leij, F.J., A. Sciortino, and A.W. Warrick. 2006. Infiltration in two parallel soil columns. Water Resour Res. 42 (12): W12408.

Lindquist, W.B., S.M. Lee, D.A. Coker, K.W. Jones, and P. Spanne. 1996. Medial axis analysis of void structure in three-dimensional tomographic images of porous media. J. Geophys. Res. 101(B4): 8297-8310.

Lindquist, W.B. and A. Venkatarangan. 1999. Investigating 3D geometry of porous media from high resolution images. Phys. Chem. Earth (A) 25: 593.

Mualem Y.A. 1976. A new model for predicting the hydraulic conductivity of unsaturated porous media. Water Resour Res. 12:513−22.

Pagliai, M., M.Raglione, T.Panini, M.Maletta, and M. Lamarca. 1995. The structure of two alluvial soils in Italy after ten years of conventional and minimum tillage. Soil Till. Res. 34 (4): 209−223.

Pagliai M. and Vignozzi N. 2002. The soil pore system as an indicator of soil quality. Advances in Geoecology, 35.

Peth, S., R. Horn, F. Beckmann, T. Donath, J. Fischer, and A.J.M. Smucker. 2008. Three-dimensional quantification of intra-aggregate pore-space features using synchrotron-radiation-based microtomography. Soil Sci. Soc. Am. J. 72(4): 897-907.

Pires, L.F., J.R. Macedo, M.D. Souza, O.O.S. Bacchi, and K. Reichardt. 2005. Gamma-ray computed tomography to investigate compaction on sewage-sludge-treated soil. Appl. Radiat. Isot. 59(1): 17−25.

Pires, L.F., M. Cooper, F.A.M. Cássaro, K. Reichardt, O.O.S. Bacchi, and N.M.P. Dias. 2008. Micromorphological analysis to characterize structure modifications of soil samples submitted to wetting and drying cycles. Catena. 72(2): 297−304.

Posadas, A.N.D., D. Gimenez, M. Bittelli, C. M. P. Vaz, and M. Flury. 2003. Multifractal characterization of soil particle-size distributions. Soil Sci. Soc. Am. J. 65(5): 1361-1367.

Radcliffe, D.E. and T.C. Ramussen. 2002. Soil water movement. In: Warrick, A.W. (ed). Soil Physics Companion. CRC Press, Boca Raton, FL.

Sheldrick, B.H. 1984. Analytical Methods Manual. LRRI Contribution No. 84−30. Agriculture Canada, Ottawa, Ontario

Sleutel, S., V. Cnudde, B. Masschaele, J. Vlassenbroek, M. Dierick, L. Van Hoorebeke, P. Jacobs, and S. De Neve. 2008. Comparison of different nano- and micro-focus X-ray computed tomography set-ups for the visualization of the soil micro-structure and soil organic matter. Comput. Geosci. 34(8): 931-938.

Spohrer, K., L. Herrmann, J.Ingwersen, and K. Stahr. 2006. Applicability of uni- and bimodal retention functions for water flow modelling in a tropical acrisol. Vadose Zone J. 5: 48−58.

Strudley, M.W., T.R. Green, and J.C. Ascough. 2008. Tillage effects on soil hydraulic properties in space and time: State of the science. Soil Till. Res. 99:4-48.

Tamboli, P.M., W.E. Larson, and M. Amemiya. 1964. Influence of aggregate size on moisture retention. Iowa Acad. Sci. 71:103-108.

Udawatta, R.P. and S.H. Anderson. 2008. CT-measured pore characteristics of surface and subsurface soils influenced by agroforestry and grass buffers. Geoderma. 145(3-4): 381-389.

Ventrella, D., N. Losavio, A.V. Vonella, and F.J. Leij. 2005. Estimating hydraulic conductivity of a fine-textured soil using tension infiltrometry. Geoderma. 124(3-4): 267-277.

Vervoort, R.W. and S.R. Cattle. 2003. Linking hydraulic conductivity and tortuosity parameters to pore space geometry and pore size distribution. J. Hydrol. 272 (1−4): 36−49.

Vogel, H.J. and K.I. Roth. 2001. Quantitative morphology and network representation of soil pore structure. Adv. Water Resour. 24(3-4):233−242.

Wittmuss, H.D. and A.P. Mazurak. 1958. Physical and chemical properties of aggregates in a Brunizem soil. Soil Sci. Soc. Am. Proc. 22:1-5.

Wosten, J.H.M. and M.T. van Genuchten. 1988. Using texture and other soil properties to predict the unsaturated soil hydraulic functions. Soil Sci. Soc. Am. J. 52:1762−1770.

Ziska, L.H., J.A. Bunce, and E.W. Goins. 2004. Characterization of an urban-rural CO2/temperature gradient and associated changes in initial plant productivity during secondary succession. Oecologia. 139 (3): 454-458.

토양 공극 형태와 수문학적 특성에 대한 3 차원적 측정

전현정 · Daniel Gimenez[1] · 윤성원[2] · Richard Heck[3] · Tom Elliot[3] · Laise Ziska[4] · Kate Geaorge[4] · 손연규 · 하상건*

농촌진흥청, 국립농업과학원 농업환경부, [1]럭거스 뉴저지 주립대학교, 환경과학과
[2]프랑스 국립 농업 연구원, [3]웰프 대학, 자원환경과, 온타리오 농과 대학, [4]농업 연구원

포어 네트웍 모델들 (Pore network model)은 토양 공극의 구조를 조사할 때 유용한 도구들이다. 이런 모델들은 삼차원 이미지들에서 공극의 구조와 관련된 양적 정보를 제공한다. 이 연구는 포어 네트웍 모델을 이용하여 공극의 구조와 수리학적 특성들을 양적으로 측정하였다. 연구목표는 큰 크기의 이미지에서 공극의 구조에 관한 양적 정보를얻기 위해 포어 네트웍 모델을 적용하고, 토양수분특성과 수리 전도도를 삼차원 이미지로부터 계산하고 이 값들은 실험을 통해 얻어진 실험값들과 결합하여 토양의 수리적 특성을 분석하는 것이었다. 토양 시료들은 발티모아 도시 중심에 있는발티모어 과학센터에 위치한 실험부지에서 채취되었다. 불교란 원주형 시료들이 채취되었고, 22 μm 의 해상도로 x선 단층 촬영되었다. 포어 네트웍은 중심축 변형에 의해 공극에서 축출되었고 이를 바탕으로 공극 구조가 계산되었다. 토양수분특성과 불포화 수리 전도도 값들은 토양 이미지에서 계산 되었다. 토양 밀도, 토양수분특성과 불포화 수리 전도도들은 3 토양 시료들로부터 실험을 통해 구하였다. 삼차원 이미지 분석은 토양 공극의 특성들을, 예를 들어 공극 부피, 길이, 굴곡도, 가장 정확히 분석하였다. 이런 정확한 분석은 토양 내 수문학적 정보를 정확히 산출할 수 있게 하였다. 계산된 값과 실험을 통한 실험치의 결합은 공극에 대한 더 광범한 범위를 분석할 수 있게 하였다. 이 연구를 통해 이미지에서 계산되고 측정된 수문학적 자료들은 토양 내 대기공과 소기공을 모두 다 설명해 줄 수 있는 방법이라는 것이 밝혀졌다.

중심어 : 공극 기하학, x선 단층 촬영, 중심축 분석, 토양수분특성, 불포화 전도도